Volume 14, Number 1, 2021. pp. 49-58

Jordan Journal of Physics

ARTICLE

Optical Properties of Cadmium Sulphide (CdS) Thin Films Spin-Coated on Glass Substrates

Osanyinlusi Oluwatoyin and **Aregbesola A. Emmanuel**

Department of Physics, University of Ilorin, Ilorin, Kwara State, Nigeria.

Doi: **https://doi.org/10.47011/14.1.5**

Received on: 17/12/2019; *Accepted on: 12/05/2020*

Abstract: CdS thin films were synthesized on a glass substrate using spin coating method. The effects of annealing temperature on the optical properties of the prepared CdS films were investigated for different annealing temperatures of 200, 300 and 400 °C. Cadmium acetate, thiourea and ammonia were used as the source materials for the preparation of the thin films. The elemental composition, morphological, optical and structural properties of the films obtained by spin coating were investigated using Energy Dispersive X- ray Spectroscopy (EDAX), Scanning Electron Microscope (SEM), UV Spectrophotometry and X-ray diffraction (XRD) respectively. The SEM image of the unannealed film shows a spherical morphology and an irregular pattern without any void. It also shows that the film covers the substrate well. Annealing leads to an increase in transmittance with the highest transmission of 87% observed for the film annealed at 400°C. With increase in annealing temperature, optical parameters like extinction coefficient and dielectric constants show a reduction, while refractive index and skin depth exhibit an improvement. The absorption coefficient increases with increasing photon energy in the range 3.6 to 4.0 eV. The band gap values of the CdS thin film samples were found to be in the range between 3.14 eV and 3.63 eV. The bandgap is somewhat greater than the value of bulk CdS due to quantum size effect. EDX image confirmed the presence of Cadmium and Sulphur in the prepared CdS films. Annealing did not significantly change the extinction coefficient. The X-ray diffraction confirms the cubic structure of CdS deposited on glass substrate, where reflections from (111), (200), (220) and (311) planes are clearly shown with a preferential orientation along (111) plane. Debye-Scherer equation was used to determine the crystallite size of the most intense plane (111) and the value was found to be 8.4 nm.

Keywords: SEM image, Spin coating, Surface morphology, Optical properties, Annealing.

Introduction

In recent years, there has been a considerable interest in thin-film semiconductors for use in solar cell devices and thin-film transistors in panel displays [1-3]

Cadmium sulfide has been the subject of intensive research because of its intermediate band gap, high absorption coefficient, reasonable conversion efficiency, stability and low cost [4-5]. Among II-VI semiconductors, cadmium sulfide (CdS) polycrystalline thin films have a wide range of applications, such as large area electronic devices and solar cells. Because of their wide direct band gap (2.42 eV), they have been used as window material together with several semiconductors, such as CdTe, Cu_2S and $CuInSe_2$ [6-7]. Cadmium sulfide has a cubic structure (zincblende), a hexagonal structure (wurtzite) or a mixture of the two according to growth deposition.

Heat treatment is often used to tune the structure and properties of thin films, such as CdS. Crystalline quality plays an important role in the utilization of the CdS films for solar cell applications. Thermal annealing leads to

Corresponding Author: Osanyinlusi Oluwatoyin **Email**: adetolusi@gmail.com

improvement in the crystalline quality of the films by the removal of strains, which can lead to phase transition, thereby changing the band gap [8].

Different methods have been used to prepare CdS, such as spray pyrolysis [9], vacuum evaporation [10], electrodeposition [11], sputtering [12], chemical bath deposition (CBD) [13], screen printing [14] and spin coating [15].

Compared to other conventional methods, spin coating has received much attention in current decades, owing to its better qualities which include low cost, ease of composition control, good film adherence, homogeneity and reproducibility of uniform films, even at shorter processing time. Moreover, the method permits molecular-level mixing and processing of raw materials and precursors at relatively lower temperatures [16 - 19]. In addition, spin coating method allows for easy deposition on different types of substrate that could be performed under non-vacuum environment [20].

In this paper, the deposition is carried out by employing an inexpensive, simplified spin coating technique on glass substrate. In addition, the optical, morphology, chemical composition and structural properties of the CdS film were studied using UV Spectrophotometry, scanning electron microscopy (SEM), EDX and X-ray diffraction (XRD).

Experimental Details

The synthesized CdS thin film samples were deposited on a glass substrate by spin coating method. A precursor solution containing Cadmium acetate ($Cd(OOCH_3)_2.2H_2O$), thiourea (H_2NCSNH_2) and Methanol was used to deposit CdS thin films. Cadmium acetate and thiourea were used as Cadmium and Sulphur precursors, respectively. Methanol was used as the solvent. All chemicals, purchased from Sigma Aldrich, were of analytical grade and used as received without any further purification. Before being used, the glass substrates were cleaned using acetone, iso-propanol and distilled water successively in an Ultrasonic cleaner and thereafter dried in air. For deposition of the films, 10 ml of 1 M Cadmium acetate was mixed with 10 ml of 1M Thiourea and stirred for 1 hour using a magnetic stirrer in order to produce a homogenous solution. The glass slide was held on the spin coating chuck at room temperature for the deposition of CdS films. The samples were prepared at a rotation speed of 1000 rpm for 30 seconds. After deposition, the films were baked in an oven at 100 °C for 30 minutes to remove the solvent and residual organics. The deposited thin films were annealed in air at temperatures of 200^0, 300^0 and 400^0C for 1 hour using a carbonite furnace. Surface morphology of the films was investigated using field emission scanning electron microscope (JEOL JSM 7600F Field emission SEM) coupled with an energy dispersion X-ray (EDX) spectrometer to confirm the elemental composition of the film. Optical transmission was carried out by Avantes-SAI-07086751 model UV Spectrophotometer in the range 300 nm to 1000 nm. The crystalline structure of the films was analyzed using a Rigaku D/Max - lllC X-ray diffractometer at a scanning rate of 2 ^{0}/min in 2 to 50^0 at room temperature with a CuKα radiation set at 40 kV and 20 mA.

Results and Discussion

Surface Morphology

Scanning Electron Microscope (SEM) was used for the surface morphology of thin film samples. The Scanning Electron Microscopy is a versatile technique for studying microstructure of thin films. The SEM images of the as prepared CdS thin film samples at different magnifications of 6000 and 10000 times are shown in Fig. 1 (a and b). The SEM image shows a spherical morphology and an irregular pattern without any voids. The film covers the substrate well. The grains are found to be thickly packed, dense, smooth and without any visible pores.

Elemental Analysis

Fig. 2 shows the energy dispersive X-ray (EDX) spectrum of the unannealed CdS thin film. The EDX spectrum confirms the presence of Cadmium (Cd) and Sulphur (S) in the thin film. The weight percentage ratio of Cd: S for the film is 55: 8, which shows that the film is Sulphur-deficient. This is similar to the result of Shaban *et al*. (2015) and may be ascribed to the higher sulphur affinity towards oxygen, so it might have converted to SO_2 and then evaporated. Also, this may be a result from the conversion of CdS to CdO during the drying at 100 °C. This may be confirmed by the existence of a strong O signal. The presence of carbon was also detected by the EDX. This may probably be from the glass substrates [21].

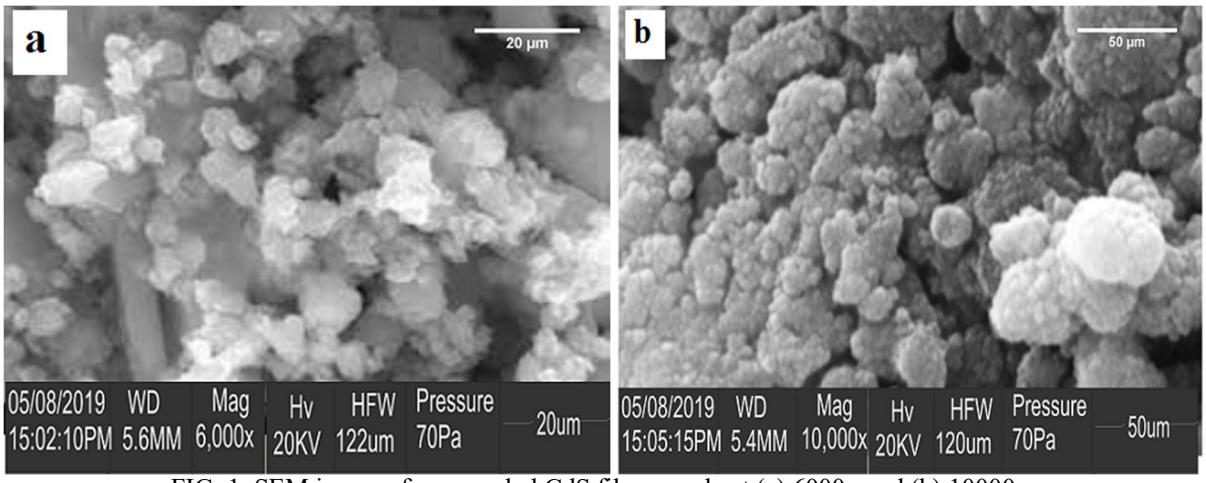

FIG. 1. SEM image of unannealed CdS film sample at (a) 6000x and (b) 10000x.

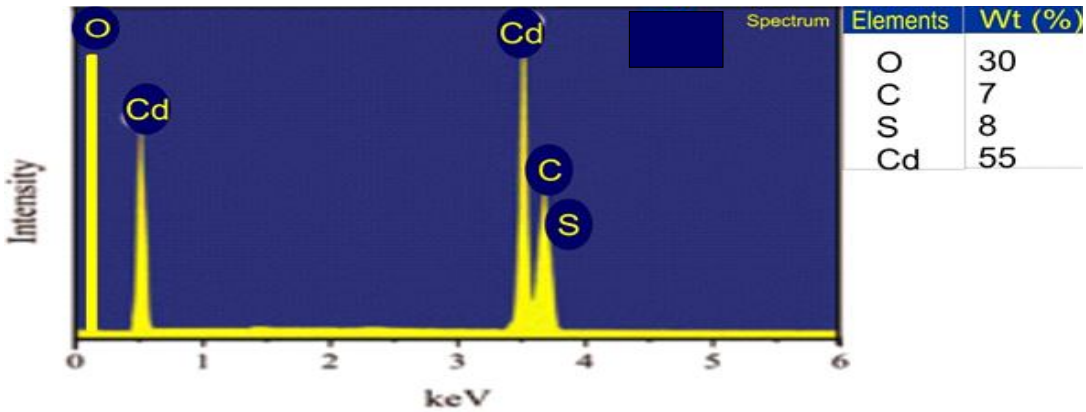

FIG. 2. EDX spectra of the CdS thin films.

Optical Characteristics

Fig. 3 shows the transmission and absorption spectra for the as deposited, 200^{0}C, 300^{0}C and 400^{0}C annealed CdS thin films. From Fig. 3a, the maximum transmissions observed are 76%, 81%, 82 % and 87 % for unannealed, 200°C, 300 ^{o}C and 400°C annealed thin films, respectively within the visible wavelength range. The observed high transmittance is one of the prerequisites for opto-electronic devices, especially solar cell window layers [22]. Beyond the visible range, the transmission remains constant for all the films. Below 400 nm, there is a sharp fall in transmission. It is clear from the figure that as the annealing temperature increases, transmittance also increase. This is in agreement with the works of Akbarnejad et al. (2017) [8] and Djelloul et al. (2016) [13]. They attributed the increase in transmittance to reduction in lattice imperfections caused by the annealing process.

The transmission data was used to calculate the absorbance of the film samples at different wavelengths using the relation [23]:

$$A = 2 - \log_{10} T \quad (1)$$

where T is the percentage transmittance and A is the absorbance.

The calculated absorption spectra are shown in Fig. 3b with the absorption remaining constant at a very low value close to zero above a wavelength of 350 nm and a sharp increase below this wavelength. The sharp increase in absorbance at the wavelength $\lambda < 350$ nm may be due to the onset of interband transitions at the fundamental edge [24]. It can be deduced from the figure that as the annealing temperature increases, the absorption decreases with the film annealed at 400^{0}C having the least absorption.

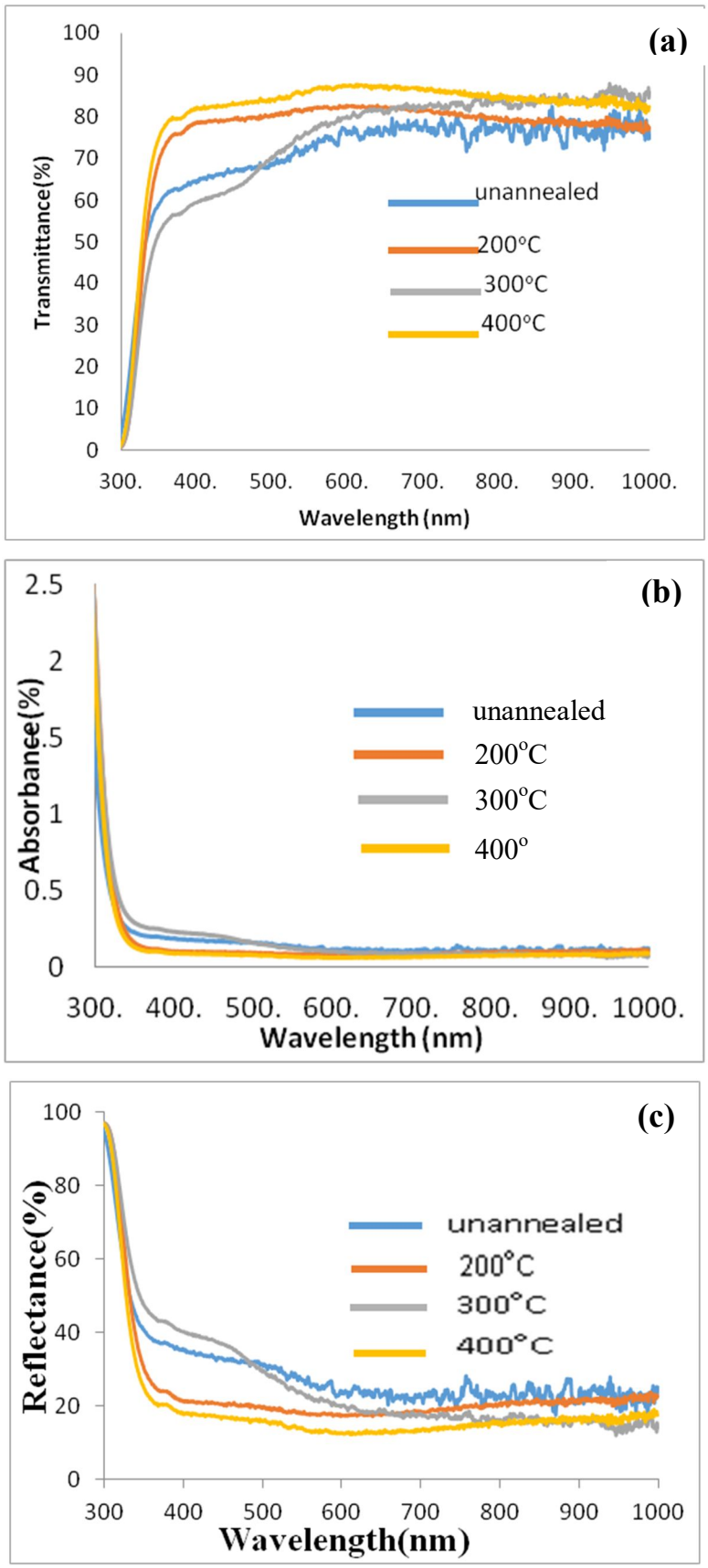

FIG. 3. (a) Transmittance (b) Absorbance and (c) Reflectance spectra for unannealed and annealed CdS thin films.

The reflectance (R) is the fraction of the incident radiation of a given wavelength that is reflected when it strikes a surface. The relation between transmittance, T (%), absorbance, A (%) and reflectance, R (%), according to the law of conservation of energy is represented by the equation below [25], from where percentage reflectance is calculated.

$$A + R + T = 100 \quad (2)$$

or

$$R = 100 - (A + T)$$

Fig. 3c shows the reflectance spectra for unannealed and annealed CdS thin films. From the plot, it is clear that an increase in annealing temperature causes a decrease in reflectance of the films with the film annealed at 400°C having the lowest reflectance of 12 % and the unannealed film having the highest reflectance of 24 % within the UV region.

The absorption coefficient was determined using Lambert equation [26]:

$$\alpha = \frac{2.303A}{t} \quad (3)$$

where A is the absorbance and t is the thickness of the film.

Fig. 4 shows the absorption coefficient as a function of photon energy. It is clear from the plot that the absorption coefficient increases with increasing photon energy in the range 3.6 and 4.0 eV.

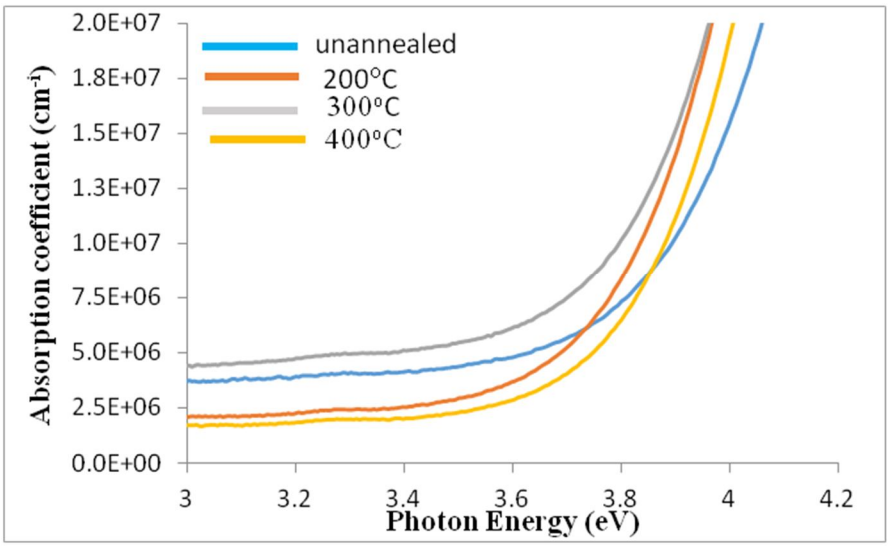

FIG. 4. Plot of absorption coefficient against photon energy for unannealed and annealed spin CdS thin films.

The energy band gap is related to the absorption coefficient (α) and can be calculated using the relation [27]:

$$(\alpha h\nu) = A\left(h\nu - E_g\right)^m \quad (4)$$

where A is a constant, E_g the energy gap, $h\nu$ the photon energy and m is ½ for direct band gap [27].

The band gap was determined by extrapolating the linear portion of the graph of $(\alpha h\nu)^2$ against $h\nu$ to α = 0, as shown in Fig. 5.

The values of the band gaps as deduced from the plot are represented in Table 1

TABLE 1. Variation of band gap with annealing temperature.

Annealing temperature (^{0}c)	Energy band gap (eV)
Unannealed	3.31
200	3.53
300	3.14
400	3.63

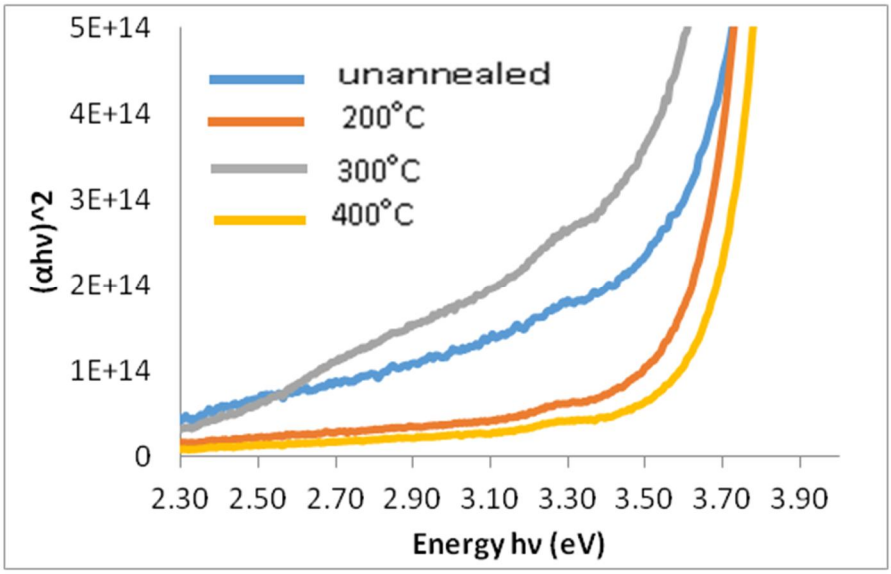

FIG. 5. Plot of $(\alpha h\nu)^2$ against $h\nu$ for unannealed and annealed CdS thin films.

The table shows that the band gap ranges between 3.14 eV and 3.63 eV. The values of the band gap are somewhat greater than the band gap of the bulk CdS (2.42 eV) [28]. These results are comparable with the results of Thambidurai *et al*. (2009) [27] and Matin *et al*. (2018) [29]. Thambidurai *et al*. found a band gap ranging between 3.56 - 3.94 eV for CdS films annealed at temperatures ranging between 150°C and 450°C [27]. Matin *et al*. (2018) found a bandgap of 2.66 eV for unannealed CdS and 3.87 eV for annealed CdS thin film at 430°C [29]. The larger bandgap may probably be due to the quantum size effect in the deposited thin films [22].

From the table, it is clear that an increase in annealing temperature results in an increase of the band gap. This is in agreement with the work of Matin *et al*. (2018) [29]. The increase in band gap after annealing can be attributed to O_2 incorporation during annealing. Similar explanation on annealed CdS thin films has been previously reported by Islam (2013) [12]. Matin *et al*. (2018) also reported that the changes of band gap with increasing annealing temperature are caused by changes in the defects, the composition and the crystalline properties of the CdS thin films.

Extinction coefficient of the CdS thin films is determined using the relation [30]:

$$k = \frac{\propto \lambda}{4\pi} \tag{5}$$

where α is the absorption coefficient, k is the extinction coefficient and λ is the incident photon wavelength.

Graph of extinction coefficient as a function of wavelength for unannealed and annealed CdS thin films is plotted in Fig. 6. The extinction coefficient values show a similar trend as the absorption coefficient. It can be observed from the figure that the values of the extinction coefficient for all the films are very close to zero. Annealing did not significantly change the extinction coefficient.

The refractive index dispersion plays a prominent part in the research of optical materials, because it is a major factor in optical communication and in designing devices for spectra dispersion. The refractive index has been determined from the reflectance data using the equation [31]:

$$n = \left[\frac{1+\sqrt{R}}{1-\sqrt{R}}\right] \tag{6}$$

where n is the refractive index and R is the reflectance.

Fig. 7 shows a plot of refractive index *versus* wavelength for unannealed and annealed CdS thin films. It is clear from the figure that all the films show an increase in refractive index as the wavelength increases within the visible region. It can also be observed from the figure that refractive index decreases with increasing annealing temperature. The maximum value of

the refractive index of 1.39 is obtained for the film annealed at 400°C at a wavelength of 611 nm.

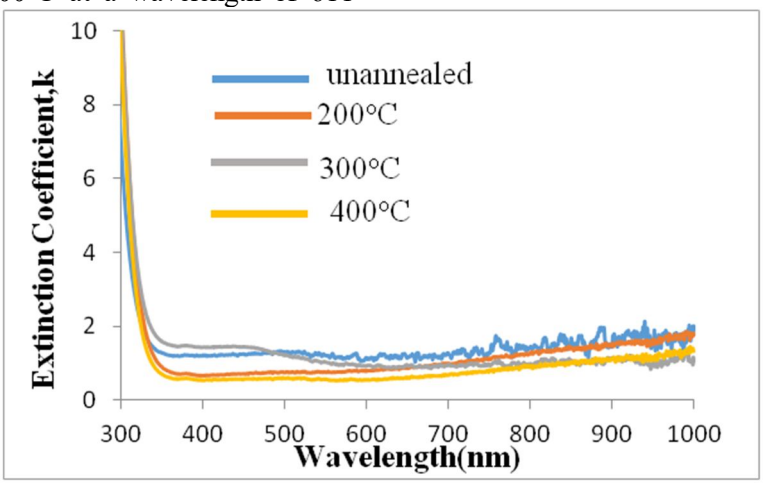

FIG. 6. Plot of extinction coefficient *versus* wavelength for unannealed and annealed CdS thin films.

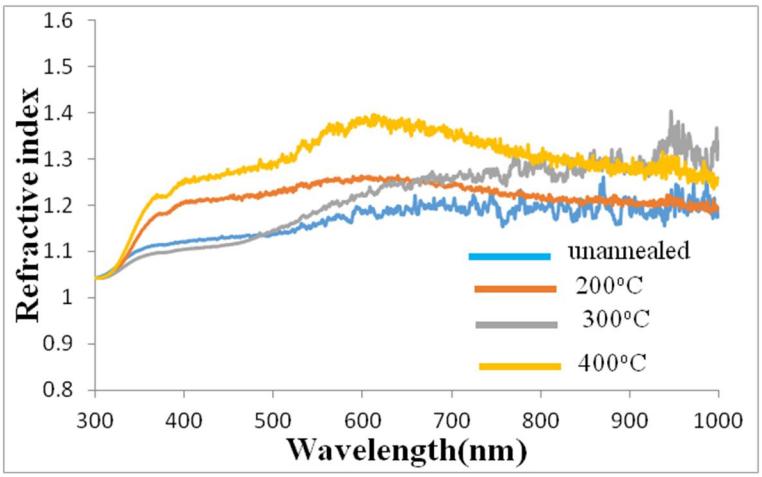

FIG. 7. Plot of refractive index against wavelength for unannealed and annealed CdS thin films.

The skin depth (χ), which represents that the electromagnetic wave will have amplitude reduced after passing through a thickness, has the formula [32]:

$$\chi = \frac{1}{\alpha} \tag{7}$$

where α is the absorption coefficient.

Fig. 8 shows a plot of skin depth against wavelength for the unannealed and annealed spin coated CdS thin films. The skin depth values show a similar trend as the transmission spectra. It can be observed from this figure that the skin depth increases with increasing wavelength within the visible region of the spectrum. It can also be deduced that the skin depth shows an increase with increasing annealing temperature.

The real and imaginary parts of the dielectric constant were determined using the relation [33]:

$$\varepsilon_c = \varepsilon_r + \varepsilon_i \tag{8}$$

where ε_r is the real part, which is the normal dielectric constant, given as:

$$\varepsilon_r = n^2 - k^2 \tag{9}$$

And ε_i is the imaginary part which represents the absorption associated with radiation by free carrier:

$$\varepsilon_i = 2nk\,. \tag{10}$$

Fig. 9 (a and b) shows the variation of real and imaginary parts of the dielectric constant with wavelength. It is clear from the figures that the dielectric constants follow the same trend as the absorption spectra. At a wavelength λ = 350 nm, both the real and imaginary parts of the dielectric constant show a sharp increase. At a wavelength λ = 350 nm, the real part (Fig. 9a) is close to zero for all the films, which remains constant throughout the range of wavelength

studied. In case of the imaginary part of the dielectric constant (Fig. 9b), the value decreases with increasing annealing temperature.

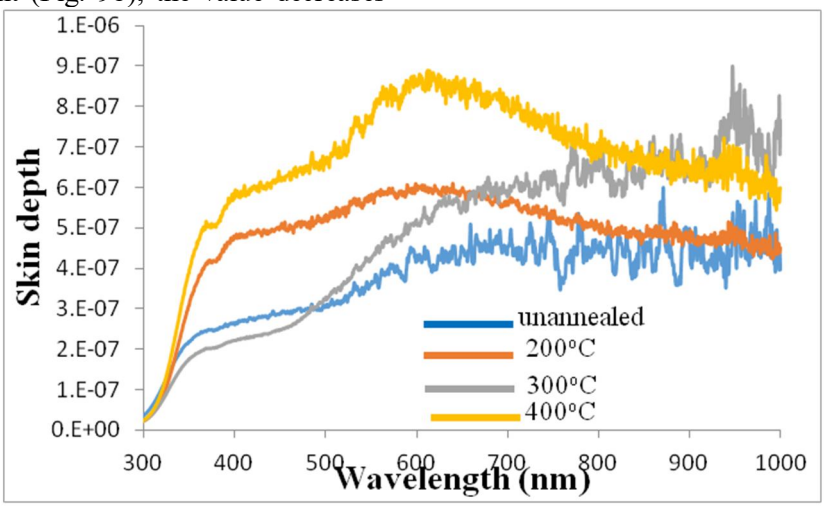

FIG. 8. Plot of skin depth against wavelength for unannealed and annealed CdS thin films.

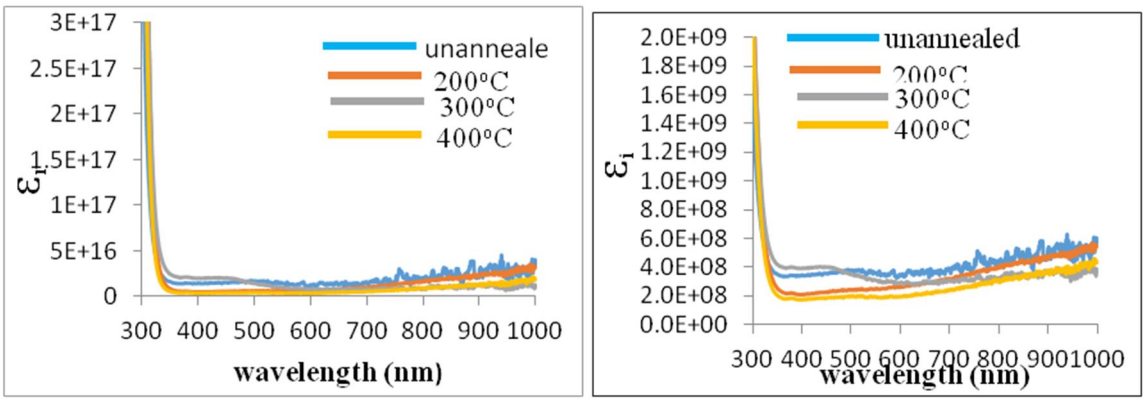

(a) (b)

FIG. 9. (a) Real part and (b) imaginary part of the dielectric constant against wavelength.

Structural Analysis

It is reported that cadmium sulfide can exist in both cubic and hexagonal forms [29]. Fig. 10 shows the XRD patterns for unannealed CdS thin films. The XRD peaks are found to be broad, indicating fine size of the sample grains [34]. From the figure, the main characteristic peaks are observed at 2θ values of 26.5, 30.8, 43.9 and 52.18°C, which correspond to (111), (200), (220) and (311) planes of cubic (zincblende) CdS, respectively. The reflections from these planes have previously been reported for CBD-CdS grown on glass substrate [35]. The observed XRD pattern are in good agreement with standard data JCPDS File No: 80-0019 [36, 37]. No peaks attributable to other phases were observed. The broadening of the diffraction peak provides information about crystallite size. As the width increases, the particle size decreases and *vice versa* [38].

From the XRD data, the crystallite size (D) was calculated using the Debye-Scherer equation [39]:

$$D = k\lambda/\beta\mathrm{Cos}\theta \quad (11)$$

where k is a constant the value of which is approximately 0.9 and it is a shape factor, θ is the Bragg angle, λ is the wavelength of the Cuk_{α} (1.5406 A) and β is the FWHM of the dominant peak in radians.

The dislocation density (δ) and the micro-strain (ε) of the unannealed CdS film were also calculated using the following relations [40]:

$$\delta = \frac{1}{D^2} \quad (12)$$

and

$$\varepsilon = \frac{\beta Cos\theta}{4}\,. \quad (13)$$

The calculated values of the crystallite size, dislocation density and micro-strain are given as

8.4 nm, 14 x 10^{15} line/m^2 and 4.2 x 10^{-3}, respectively. Marin *et al*. (2018) [29] has reported a crystallite value of 5.62 nm for chemically deposited CdS. Oztaş et al. (2018) [41] reported a value of micro-strain of 4.3 x 10^{-3} for CdS thin film prepared by spray pyrolysis.

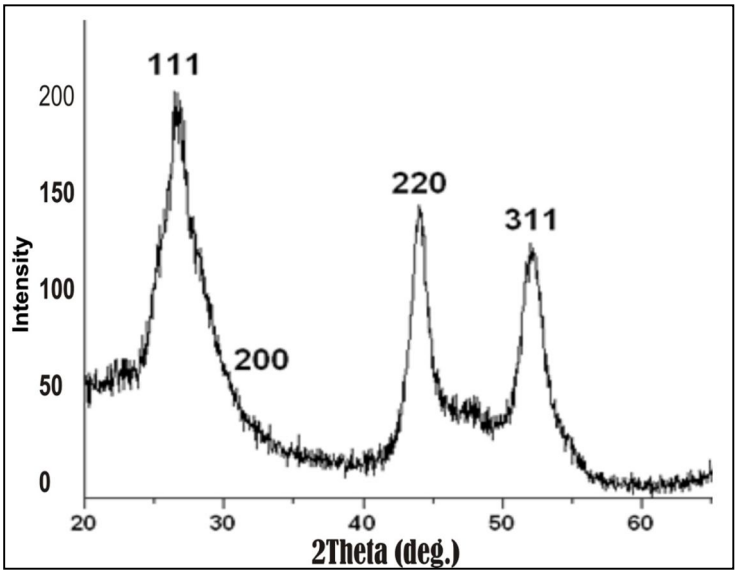

Figure 10: XRD pattern of unannealed CdS thin films.

Conclusion

Cadmium sulphide thin films were synthesized using spin coating method and studied at different annealing temperatures. From the optical analysis of the films, it is clear that an increase in annealing temperature brought about an increase in transmittance. The highest transmittance recorded is 87% and it is associated with the annealing temperature of 400^0C. The absorbance decreases with increase in annealing temperature. Optical parameters, like extinction coefficient and dielectric constant show a reduction with increasing annealing temperature while refractive index and skin depth exhibit an improvement with increasing annealing temperature. The SEM result shows that the surface of the deposited CdS thin film has a spherical morphology and an irregular pattern without any voids. The elemental analysis also reveals the presence of Cadmium and Sulphur in the thin film. From the XRD analysis, it is observed that the prepared films have a cubic structure. The broadening of the diffraction peak provides information about crystallite size. As the width increases, the particle size decreases and *vice versa*. The band gap values range between 3.14 eV and 3.63 eV, which were somewhat larger than the typical value of the bulk CdS (2.42eV). This could be attributed to quantum confinement effects. This study revealed that CdS has a significant potential for use as a window layer in photovoltaic devices.

References

[1] Bonnet, D., Proc. of 19th European PV Solar Energy Conf., WIP-Munich and ETA-Florence, 2 (2004) 1657.

[2] Abu-Safe, H.H., Hossain, M., Naseem, H., Brown, W. and Al-Dhafiri, A., J. Elec. Mater., 33 (2) (2004) 128.

[3] Savadogo, O., Sol. Ener. Mater. Sol. Cells, 52 (1998) 361.

[4] Romeo, N., Bosio, A., Canevari, V., Podesta, A., Mazzamuto, S. and Guadalupi, G.M., Proc. of 19th European PV Solar Energy Conf., WIP-Munich and ETA-Florence, 2 (2004) 1718.

[5] Krunks, M., Madarasz, J., Hiltunen, L., Mannonen, R., Mellikov, E. and Niinisto, L., Acta. Chem. Scand., 51 (1997) 294.

[6] Mirkamali, A., J. Opt. Nan., 1 (2017) 31.

[7] Daranfed, W., Aida, M., Attaf, N., Bougdira, J. and Rinnert, H., J. Alloys Compd., 542 (2012) 22.

[8] Akbarnejad, E., Ghorannevis, Z., Abbasi, F. and Ghoranneviss, M., J. Theor. Appl. Phys., 11 (2017) 45.

[9] Ashour, A., Turk. J. Phys., 27 (2003) 551.

[10] Mahmoud, S.A., Ibrahim, A.A. and Riad, A.S., Th. Sol. Fil., 372 (2000) 144.

[11] Mahanama, G.D.K., Madarasinghe, D.A., Dharmaratna, W.G.D. and Jayasundara, D., Ruh. J. Sci., 9 (2018) 57.

[12] Islam, M.A., Hossain, M.S., Aliyu, M.M., Chelvanathan, P., Huda, Q., Karim, M.R., Sopian, K. and Amin, N., Energy Proc., 33 (2013) 203.

[13] Djelloul, A., Adnane, M., Larbah, Y., Zerdali, M., Zegadi, C. and Messaoud, A., J. Nan. and Elect. Phys., 8 (2) (2016) 02005.

[14] Kumar, V., Sharma, D.K., Bansal, M.K. and Dwivedi, D.K, Science of Sintering, 43 (3) (2011) 335.

[15] Shaban, M., Mustafa, M. and Hamdy, H., J. Appl. Phys., 7 (6) (2015) 19.

[16] Curran, M.D. and Stiegman, A.E., J. of Non-Cryst. Sol., 249 (1999) 62.

[17] Hamideh, S.J., Int. J. Thin Film Sci. Tec., 2 (3) (2013) 1.

[18] Roy, B., Perkins, J.D., Kaydanova, T., Young, D.L., Taylor, M., Miedaner, A., Curtis, C., Kleebe, H.J., Readey, D.W. and Ginley, D.S., Thin Solid Films, 516 (2008) 4093.

[19] DiLuccio, T., Piscopiello, E., Laera, A.M. and Antisar, M.V., Mater. Sci. Eng., 27 (2007) 1372.

[20] Hashim, H., Shariffudin, S.S., Saad, P.S.M. and Ridah, H.A.M., IOP Conf. Series: Mat. Sci. and Eng., 99 (2015) 012032.

[21] Xavier, R.J., Prema, A.A., Sahayaraj, P.A., Pragathiswaran, C. and Dharmalingam, V., Adv. Appl. Sci. Res., 7 (2) (2016) 178.

[22] Shanmugavadivu, R.A., Yuvaloshini, J. and Ravi, G., Int. J. Semicond. Sci. & Tech., 3 (2) (2013) 33.

[23] Roy, R., Choudhary, V.S., Patra, M.K. and Pandya, A., J. Opt. and Adv. Mat., 8 (4) (2006) 1352.

[24] Elmas, S., Ozcan, S., Ozder, S. and Bilgin, V., Acta. Phys. Pol. A, 121 (2012) 56.

[25] Prabahar, S., Suryanarayanan, N. and Kathirvel, D., Chal. Lett., 6 (2009) 577.

[26] Yakuphanoglua, F., Viswanathan, C., Peranantham, P. and Soundarrajan, D., J. Optoelect. Adv. Mat., 11 (7) (2009) 945.

[27] Thambidurai, M., Murugan, N., Muthukumarasamy, N., Vasantha, S., Balasundaraprabhu, R. and Agilan, S., Chal. Lett., 6 (4) (2009) 171.

[28] Enriques, J. and Mathew, X., Solar Energy Mater. Solar Cells, 76 (2003) 313.

[29] Matin, R., Bashar, M.S., Sultana, M., Ahmed, A.N. and Gafur, A., Int. J. Nanoelect. and Mat., 11 (2) (2018) 221.

[30] Hamisi, N.A. and Johan, M.R., Int. J. Elect. Sci., 7 (2012) 8458.

[31] Abdullah, M.T, Ahmad, A.S.S. and Mohammed, A.A., Adv. Mat. Phys. and Chem., 5 (2015) 140.

[32] Solieman, A.S., Hafiz, M.M., Abu-Sehly, A.A. and Alfaqeer, A.A., J. Taibah Univ. Sci. 8 (2014) 282.

[33] Chopra, K.L., "Thin Film Phenomena", (McGraw Hill BooK Company, USA, 1969).

[34] Moualkia, H., Hariech, S. and Aida, M.S., Thin Solid Films, 518 (2009) 1259.

[35] Oladeji, I.O., Chow, L., Liu, J.R., Chu, W.K., Bustamante, A.N.P., Fredricksen, C. and Schulte, A.F., Thin Solid Films, 359 (2000) 154.

[36] Rajpal, S. and Bandyopadhyay, V., J. Nan. and Electr. Physics, 5 (3) (2013) 03021.

[37] Al-Hussam, A.M.A. and Jassim, S.A., J. Ass. Arab Univer. for Basic and Applied Sciences, 11 (1) (2012) 27.

[38] Banerjee, R., Jayakrishnan, R. and Ayyub, P., J. Phys. Condens. Matt., 12 (2000) 10647.

[39] Jeorg, J., Choi, S.P., Hong, K.J., Song, H.J. and Park, J.S., J. Korean Phys. SCO, 48 (2006) 960.

[40] Senthilarasu, S., Sathyamoorthy, R. and Lalitha, S., Sol. Energy. Mater. Sol. Cells, 82 (2004) 299.

[41] Oztas, M., Bedir, M., Haciibrahimoglu, M.Y., Ozdemir, Y. and Mert, S., Nanomed. Nanotechnol., 3 (1) (2018) 000130.